# Modeling of Gan-MOSHEMT for Use in a High-Frequency Application

Fatma M. Mahmoud<sup>1</sup>, \*, Amira Nabil<sup>2</sup>, Mohamed Abouelatta<sup>3</sup>, Gamal M. Dousoky<sup>1</sup>, and Mahmoud A. Abdelghany<sup>1</sup>

<sup>1</sup>Department of Electrical Engineering, Faculty of Engineering, Minia University, Minia 61517, Egypt
<sup>2</sup>Department of Electronics and Communications, Higher Institute for Engineering and Technology, New Cairo,
Egypt

<sup>3</sup>Department of Electronics and Communications, Faculty of Engineering, Ain Shams University, Cairo 11517, Egypt

#### **Abstract**

The calibration, modeling, and simulation of Metal-Oxide-Semiconductor High-Electron Mobility Transistors (MOSHEMTs) based on the AlGaN/GaN material system are presented in detail in this research. With the use of the Sentaurus Technology computer-aided design (TCAD) tool, the device was calibrated and simulated. The effect of gate length on the frequency response of the device has been presented. We used the LTSPICE software to simulate the GaN-MOSHEMT using typical MOSFET equations and their corresponding parameters. The validation of our model was made possible by the following comparison of simulation results obtained from our model with TCAD Sentaurus outcomes. According to the results, an achievable device model helps to design many circuits in high-frequency and power electronics.

Keywords: GaN, MOSHEMT, Cut-off frequency, Modeling, MOSFET equations, LTSPICE.

#### 1. Introduction

The The field of semiconductor materials, particularly Group III-nitrides like GaN, has captured significant attention in various industries due to inherent properties, making exceptionally well-suited for applications in optoelectronics, high-frequency electronics, and high-power scenarios. These materials, which include GaAs, GaN, and SiC, have proven their superiority over silicon in radio-frequency (RF) and microwave applications [Josef et al., 2011, JADLI et al., 2021, Fletchera et al., 2017]. In particular, GaN/AlGaN heterostructure devices have found their niche in high-power microwave applications, capitalizing on the substantial bandgap offset at the Al-GaN/GaN interface and the presence of charges generated by spontaneous and piezoelectric polarization. These factors combine to enhance carrier mobility within the channel, catering to the requirements of fast electronic applications [Ambacher et al., 1999].

With the increasing interest in GaN-HEMTs for high-power and high-frequency circuits, researchers are actively exploring various device models [Mantooth et al., 2015, Endruschat et al., 2019, Santi et al., 2015]. As a result, there is a growing need for simplified and effective GaN-HEMT modeling techniques to facilitate high-frequency system

simulations. In the literature, multiple modeling approaches for GaN-HEMTs can be found, broadly classified into four categories: behavioral models, semiphysics-based models, physics-based models, and numerical models [Mantooth et al., 2015, Santi et al., 2015, Li et al., 2017]. Semiphysics-based models, in particular, serve as a bridge between behavioral equations and semiconductor physics, offering a balance between accuracy and computational efficiency [Shah et al., 2012, Aghdam et al., 2015, Huang et al., 2014, DasGupta et al., 1998]. In line with this, our paper employs a semiphysics-based model integrated within the Simulation Program with Integrated Circuit Emphasis (SPICE) to accurately model GaN-HEMTs. In this work, we calibrated the structure of GaN-MOSHEMT via TCAD Sentaurus. Extracting SPICE parameters by using MOSFET equations and verifying (IDS-VGS) and (IDS-VDS) curves in LTSPICE are performed to make a spice model and simulate the frequency response of the proposed model, which is closed with the result of TCAD Sentaurus. The effect of the gate length on the frequency performance of the device is discussed.

The paper is structured as follows: In Section 2, we offer a device description of AlGaN/GaN MOSHEMT. Section 3 outlines the process of device calibration; while Section 4 discusses geometrical

parameters analysis Section 5 introduce the extraction of SPICE parameters for the device. Section 6 is dedicated to the validation of experimental characteristics in LTSPICE. Finally, Section 7 will draw conclusions and summarize the key findings of this paper.

#### 2. Device description

The configuration used for the simulation is visually represented in Figure 1 [Edwin et al., 2012]. In this structure, both L s-g and L d-g lengths are precisely set at 500 nm. The drain and source regions are meticulously designed with an ohmic contact, exhibiting a remarkably high n-doped concentration of  $1 \times 10^{20}$ /cm-3. Furthermore, the gate length is maintained at 300 nm. featuring a work function of 4.4 eV. The AlGaN/GaN MOSHEMT structure encompasses a 20-nm AlGaN barrier coupled with a 2 µm thick GaN layer. This specific AlGaN/GaN heterostructure configuration plays a pivotal role in facilitating the formation of a two-dimensional electron gas (2DEG) along the AlGaN/GaN interface [Nifa et al., 2017, Nifa et al., 2019]. The actual 2DEG formation primarily transpires within the lower bandgap GaN layer at this interface, which is n-type doped with a concentration of  $1 \times 10^{16}$  cm<sup>-3</sup>. The gate dielectric material employed for the simulation is Al<sub>2</sub>O<sub>3</sub>, distinguished by its 8.7 eV bandgap and a notably high dielectric constant value of 9. The gate dielectric thickness is finely tuned to 7 nm [Verma et al., 2020].

The polarization effect within the AlGaN/GaN heterostructure is a fundamental factor influencing the formation of 2DEG [Edwin et al., 2012]. This effect is carefully considered across all structure interfaces, and polarization charge calculations are executed as per the established method [Wood et al., 2007]. The substantial difference in thickness between the GaN and AlGaN layers, the GaN layer assumed to be completely relaxed, predominantly exhibiting spontaneous polarization [Edwin et al., 2012]. This spontaneous polarization effect results from the non-centrally symmetric structure inherent in GaN. Notably, spontaneous polarization also exists within AlGaN, albeit with a differing magnitude from that observed in GaN. The con-trast in the spontaneous polarization characteristics of GaN and AlGaN serves as one of the primary sources contributing to the formation

of 2DEG. Additionally, piezoelectric polarization emerges as a result of the strain or stress induced within the crystal lattice due to physical distortion when layers are interconnected at the heterojunction interface.

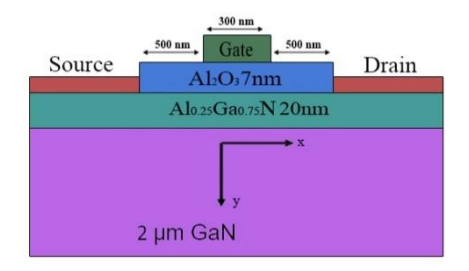


Fig.1: Structure used in the simulation [Edwin et al., 2012]

#### 3. Device calibration

Before the calibration process for the High-Electron-Mobility Transistor (HFET) structure, as illustrated in Figure 1, is carried out through the utilization of TCAD Sentaurus. Within this calibration endeavor, four distinct mobility models are harnessed in the simulation: the Masetti model (which accounts for doping-dependent mobility), the constant-mobility model, the Canali model (considering high-field-saturation mobility), and the Lombardi model (addressing interface-degradation mobility) [Edwin et al., 2012]. During the TCAD simulation, default parameters are maintained, featuring a 25% mole fraction within the AlGaN layer, a 20 nm thickness for the AlGaN layer, a dielectric constant of 9.8, an electron mobility of 1200 [cm<sup>2</sup>/Vs], and a 3.4 [eV] bandgap for GaN.

The simulation outcomes undergo meticulous calibration, meticulously referencing the experimental data collected in [Shah et al., 2012, Liu et al., 2010]. Figure 2, 3 provides a graphical representation of the I<sub>DS</sub>–V<sub>GS</sub>, I<sub>DS</sub>–V<sub>DS</sub> relationship, alongside the corresponding experimental data. Notably, the simulated results exhibit a commendable alignment with the experimental measurements, affirming the effectiveness of the calibration process.

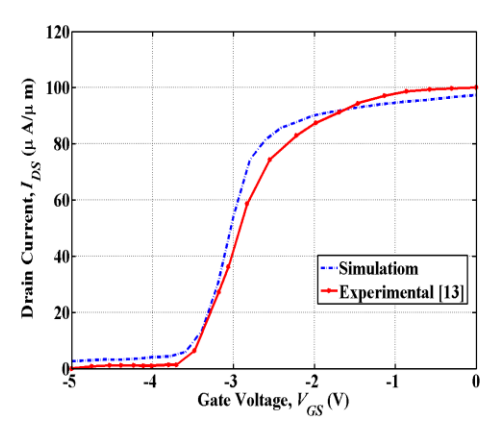


Fig. 2: Calibrated IDS-VGS of AlGaN/GaN MOSHEMT [Edwin et al., 2012]

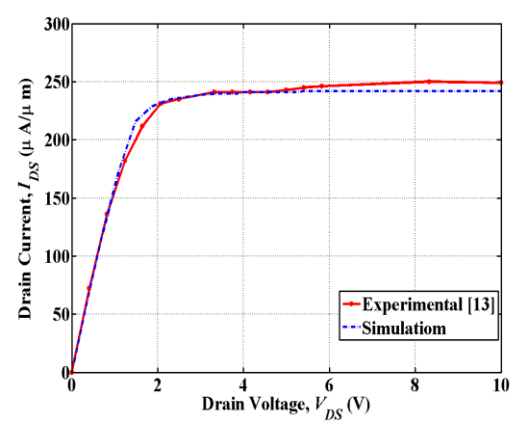


Fig.3: Calibrated IDS-VDS of AlGaN/GaN MOSHEMT [Edwin et al., 2012]

## 4. Geometrical parameters analysis

To be acceptable in high-fast and large-power applications, the cutoff frequency  $f_t$  determines the RF achievement of any transistor design [Islam et al., 2022, Jabbar et al., 2022].

The relationship between gm and  $f_t$  is important for improving the cutoff frequency. Transconductance is defined as the differentiation of the drain current with respect to the gate voltage at a constant drain voltage. The electron velocity and charge density at the contact rise as the electric field increases, leading in improved  $g_m$ . The device sensitivity is enhanced by high drain current, strong carrier concentration, and good transconductance. A high transconductance rating indicates that the device is fast and has a high drain current. The capacitance total is calculated as follows:

$$C_{\rm gg} = C_{\rm gd} + C_{\rm gs} \tag{1}$$

The capacitance between the gate and drain is indicated as  $C_{\rm gd}$ , whereas that between the gate and source is indicated as  $C_{\rm gs}$ .  $C_{\rm gg}$  affects the power

dissipation and switching behavior.  $C_{\rm gg}$  and  $g_m$  influence the cut-off frequency. Cut-off frequency  $f_t$  is inversely proportional to gate capacitance  $C_{\rm gg}$  [Rao et al., 2021]. To improve the high-frequency performance of HEMTs, smaller values of  $C_{\rm gs}$  and  $C_{\rm gd}$  are required.  $f_t$  can be calculated as follows:

$$f_t = \frac{g_m}{2\pi \left(C_{\rm gs} + C_{\rm gd}\right)} \quad (2)$$

#### 4.1 Effect the gate length, Lg

Gate lengths used in this simulation are 400 and 300 nm. The effects of  $L_{\rm g}$  variation on ft are shown in Figure 4. It clearly shows that decreasing  $L_{\rm g}$  results in an increase in  $f_t$  up to its maximum value of about 16 GHz at  $L_{\rm g}$  = 300 nm. Because  $f_t$  is inversely related to the gate capacitance, a reduction in the gate length results in a significant reduction in the gate capacitance, which leads to a significant improvement in the AC characteristics.

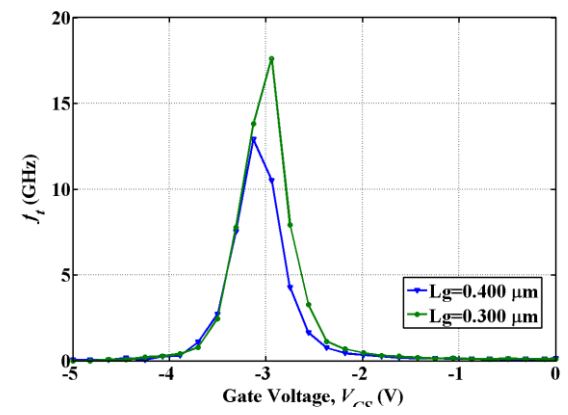


Fig.4: ft versus VGS at different Lg values

# 5. Extraction spice parameters for the device model

To effectively model a GaN-HEMT, it is essential to derive mathematical expressions that describe the drain current (IDS) concerning the applied VGS and VDS voltages. Within the SPICE framework, various sets of equations, referred to as model levels, are available for this purpose. When considering modeling GaN-HEMTs, MOSFET LEVEL 3 emerges as a significantly superior choice compared to MOSFET LEVEL 1 due to its nearly equal simplicity and enhanced accuracy [JADLI et al., 2021].

In our GaN-HEMT modeling, equations (3) and (4) sourced from the relatively more complex MOSFET LEVEL 3 model are employed. The vital SPICE parameters necessary to activate this choice are denoted in bold type. This list includes the

transconductance parameter (KP), threshold voltage (Vto), channel length (L), channel width (W), drain resistance (Rd), source resistance (Rs), body-effect parameter (Gamma), surface potential in strong inversion (Phi), and the mobility modulation constant (Theta) [Dimitrijev et al., 2012]. Particularly, the default settings of the remaining SPICE parameters render all other equations inactive [JADLI et al., 2021].

$$I_{DS} = \frac{KP}{1 + Theta(V_{GS} - V_{to})} \frac{W}{L} (V_{DS} - R_s I_D - RdI_D) - \left[1 + \frac{Gamma}{2\sqrt{Phi}}\right] \frac{(V_{DS} - R_s I_D)^2}{2}$$
 Triode Region (3)

$$I_{DS} = \frac{KP}{1 + Theta(V_{GS} - V_{to})} \frac{W}{L} \left[ \frac{2\sqrt{Phi}}{2(2\sqrt{Phi} + Gamma)} \right] (V_{GS} - V_{to})^{2} \times Saturation Region$$
 (4)

The process of extracting initial parameter values for MOSFET Level 3 involves key parameters, namely KP, Vto, Rs, and Rd. By maintaining their typical or default values during the process of nonlinear fitting, we have the flexibility to modify the values of the remaining parameters. To facilitate this, the transfer characteristics of the corresponding GaN-MOSHEMT, as detailed in [13], which involve multiplying the drain current by 1  $\mu m$ to determine the total drain current, become instrumental in the computation of KP and Vto. In line with the discussion found in reference [Islam et al., 2022], it's important to note that the values of Theta ( $V_{GS}$ -Vto),  $RsI_D$ , and  $RdI_D$  are negligible within the linear portion of the transfer characteristic, as indicated by the line in Figure 5. This simplifies equation (1) into the following linear form:

$$I_{DS}=KP(W/L)(V_{GS}-V_{to})V_{DS}$$
 (5)

Equation (5) demonstrates that Vto = (-3.5) V is the point at which the extrapolated linear section of the measured transfer characteristic intersects the VGS axis. For VDS = .5V, W =1 $\mu$  m, and L = 0.3 $\mu$  m, the slope of the linear section is (2e-4) A/V, which translates to KP = (1.2e-4) A/V2.

As shown in the reference [22], we can calculate Rs and Rd using the equation below:

$$Rs + Rd = \frac{VDS}{ID} - \frac{1}{\left(\frac{IDS}{VDS}\right) + \beta \Delta VG}$$
(6)

where,  $\beta = KP(\frac{W}{L})$ , For the specific data shown in Figure 2,  $\Delta VG = (0.5)$  V,  $V_{DS} = 0.5$  V, and  $I_{DS} = (100\mu\text{A})$ . For simplification of the model, we assume equal drain and source resistances, which are Rs = Rd = 1250 $\Omega$ .

The energy gap of the material determines the value of Phi, according to semiconductor physics. We can set Phi = 2 V for the GaN instance. Gamma = 0 in SPICE, which is the default value for this purpose, might be used as the starting point. Theta = 0 is also the parameter's default value in SPICE. This works well as the starting point for the nonlinear fitting, which modifies the theta value's final value to better fit the transfer and output characteristics. Finally, take note that the subthreshold current can be fitted to the transfer characteristic by specifying the NFS parameter. This characteristic typically has a value of 10<sup>11</sup> cm<sup>-2</sup>. However, as can be seen from Equations (3) and (4), the NFS has no impact on the IDS in the triode and saturation area. Therefore, after the non-linear fitting is finished, the value of this parameter can be changed in the SPICE simulation [JADLI et al., 2021].

### 6. Spice simulation

To validate the effectiveness of the parameter modeling, a simple circuit, as depicted in Figure 6 [Garcia et al., 2018], was employed. The gate-tosource and drain-to-source voltages underwent sweeping within the ranges of -5 to 0 V and 0 to 10 V, respectively. Utilizing the predefined values of W = 1  $\mu$ m, L = 0.3  $\mu$ m, and Phi = 2 V, in conjunction with the initial parameter values obtained in the preceding subsection (KP, Vto, Rs, Rd, Cgso, and Cgdo), the optimization process focused on refining KP, Cgso, and Cgdo to align with the desired curves. The simulated  $V_{GS}$ - $I_{DS}$  and  $V_{DS}$ - $I_{DS}$  curves for the GaN-MOSHEMT, as illustrated in Figures 7 and 8, were generated, which are closed with the results of Figures 2 and 3. Moreover, Figure 9 clearly demonstrates a remarkable alignment in frequency response simulations between TCAD SENTURUS and LTSPICE, particularly in the frequency range exceeding 16 GHz and falling below 20 GHz. Hence, it is clear that the used MOSFET LEVEL 3 equations in SPICE can be utilized to model GaN-MOSHEMTs because they have a good agreement with figure 3,4 and the measured results in [Liu et al., 2010].

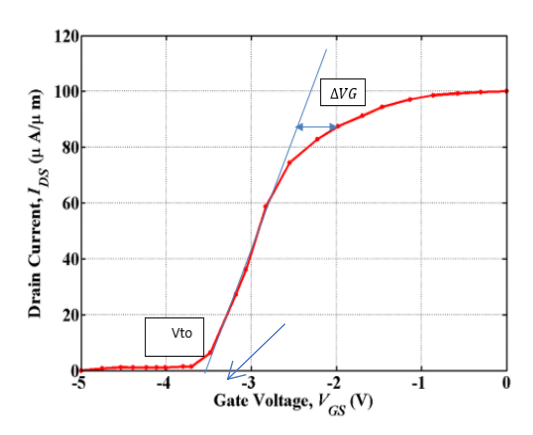


Fig. 5: Extraction of KP, Vto, Rs, and Rd from transfer characteristic GaN-MOS HEMT.

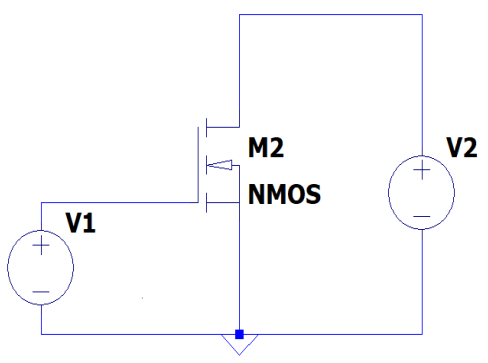


Fig.6: Circuit implemented in SPICE for parameter sweep.

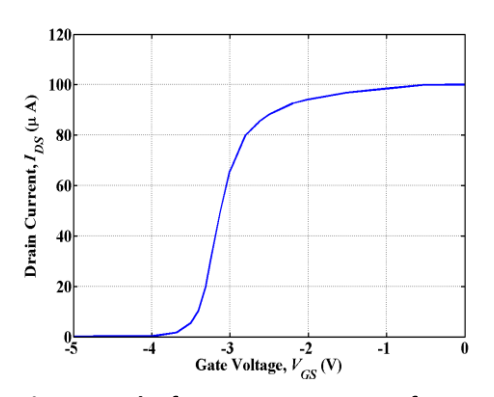


Fig.7: Results for parameter sweep for IDS versus VGS in LTSPICE.

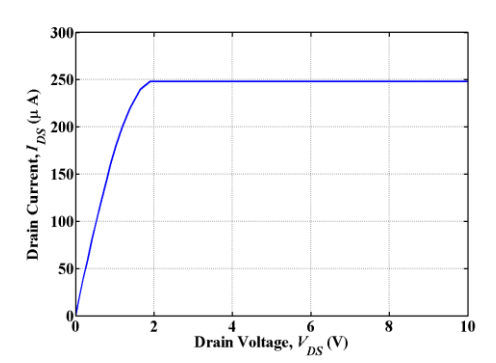
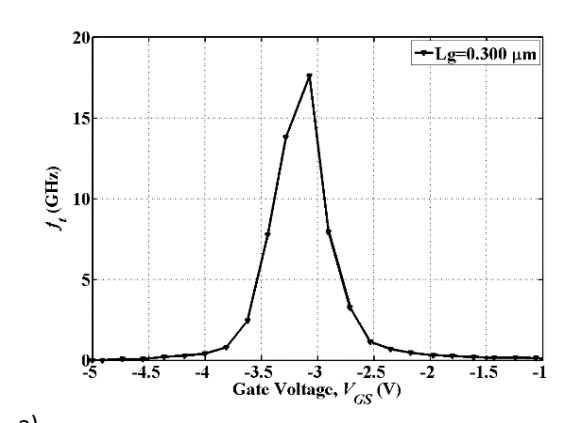


Fig. 8: Results for parameter sweep for IDS versus VDS in LTSPICE



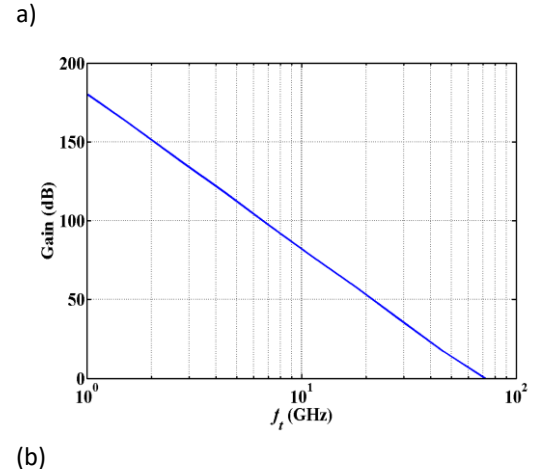


Fig.9: Frequency response for GaN- MOSHEMT at Lg=300nm (a) simulation in TCAD senturus (b) simulation in LTSPICE at VGS=-3.2 V.

#### 7. Conclusion

The included calibration of an AlGaN/GaN MOSHET usi-ng the reliable Sentaurus TCAD tool was the focus of this research project. The GaN MOSHEMT modeling procedure was carried out by utilizing SPICE parameters, which were carefully retrieved from MOSFET equations and then verified by comparing I-V curves. The frequencies obtained in TCAD Sentaurus were very similar to those found in LTSPICE, particularly in the 16 GHz - 20 GHz frequency range. Together, our results highlight the AlGaN/GaN MOSHEMT's great potential in the field and validate it as a very viable choice for high-frequency applications.

**Author contributions**: All the authors have accepted responsibility for the entire content of this submitted manuscript and approved submission.

Research funding: None declared.

**Conflict of interest statement**: The authors declare no conflicts of interest regarding this article

#### 8. References

- [1] Josef L., Heinrich S., Uwe S. (2011). Rik, Semiconductor Power Devices: Physics, Characteristics, Reliability, Springer Science & Business Media.
- [2] JADLI, U. (2021). Modeling Power GaN-HEMTs Using Standard MOSFET Equations and Parameters in SPICE. Electronics, 10.2: 130.
- Fletchera A.S, Nirmal D. (2017). A Survey of Gallium Nitrate HEMT for RF and High Power Applications, Superlattices and Microstructures, 109,519-537.
- Ambacher O., Smart J., Shealy J.R., Weimann N.G., Chu K., Murphy M. et al. (1999). Stutzmann, Twodimensional electron gases induced spontaneous and piezoelectric polarization charges in N- and Ga-face AlGaN/GaN heterostructures. Journal of applied physics, 85, 3222-3233.
- [5] Mantooth, H.A., Peng K, Santi E, Hudgins J.L. (2015). Modeling of Wide Bandgap Power Semiconductor Devices—Part I. IEEE Trans. Electron Devices, 62, 423-433.
- [6] Endruschat, A, Novak, C, Gerstner, H, Heckel, T, Joffe, C, März, M. (2019). A Universal SPICE Field-Effect Transistor Model Applied on SiC and GaN Transistors. IEEE Trans. Power Electron, 34, 9131- [18] Liu X., Liu B., Low E. K. F., Chin H.-C., Liu W., Yang 9145.
- [7] Santi, E, Peng, K, Mantooth, H.A, Hudgins, J.L. (2015). Modeling of Wide-Bandgap Semiconductor Devices—Part II. IEEE Trans. Electron Devices, 62, 434-444.
- Li, H, Zhao, X, Su, W, Sun, K, You, X, Zheng, T.Q. (2017). Nonsegmented PSpice Circuit Model of GaN HEMT with Simulation Convergence Consideration. IEEE Trans. Ind. Electron, 64, 8992-9000.
- [9] Shah, K.; Shenai, K. (2012). Simple and Accurate Circuit Simulation Model for Gallium Nitride Power Transistors. IEEE Trans. Electron Devices, 59, 2735- [20] Jabbar W. A., Mahmood A., Sultan J. (2022). 2741.
- [10] Aghdam, G.H. (2015). Model characterization and performance evaluation of GaN FET in DC-DC POL regulators. In Proceedings of the 2015 IEEE International Telecommunications Energy Conference (INTELEC), Osaka, Japan, 18-22 October, 1-4.
- [11] Huang, X, Li, Q, Liu, Z, Lee, F.C. (2014). Analytical loss model of high voltage GaN hemtin cascode configuration. IEEE Trans. Power Electron, 29, 2208-2219.

- [12] DasGupta, N, DasGupta, A. (1998). A new SPICE MOSFET Level 3-like model of HEMT's for circuit simulation. IEEE Trans. Electron Devices, 45, 1494-1500.
- [13] Edwin L.K. (2012). Characterization and Numerical Simulation of Gallium Nitride-Based Metal-Oxide-Semiconductor High Electron Mobility Transistor with High-K Gate Stack. Master Thesis, National University of Singapore.
- [14] Nifa I., Leroux C., Torres A., Charles M., Blachier D. Reimbold G, et al. (2017). Characterization of 2DEG in AlGaN/GaN heterostructure by Hall effect, Microelectronic Engineering, 178,128-131.
- [15] Nifa I., Leroux C., Torres A., Charles M., Reimbold G., Ghibaudo G. (2019). Characterization and modeling of 2DEG mobility in AlGaN/AlN/GaN MIS-HEMT, Microelectronic Engineering, 215, 110976.
- [16] Verma M& Nandi A. (2020). Design and Analysis of AlGaN/GaN Based DG MOSHEMT for High-Frequency Application, Transactions on Electrical and Electronic Materials, 21, 427-435.
- [17] Wood C & Jena D. (2007). Polarization effects in semiconductors: from ab initio theory to device applications. Springer Science & Business Media.
- M. et al. (2010). Diamond-like carbon (DLC) liner with highly compressive stress formed AlGaN/GaN MOS-HEMTs with in situ silane surface passivation for performance enhancement, IEEE International Electron Device Meeting, Francisco CA, 11.3.1 - 11.3.4.
- [19] Islam N., Mohamed M. F. P., Khan M. F. A. J. et al. (2022). Reliability, applications and challenges of GaN HEMT technology for modern power devices: A review, Crystals, 12: 11, https://doi.org/ 10.3390/cryst12111581
- Modeling and characterization of optimal nanoscale channel dimensions for fin field effect transistor based on constituent semiconductor materials. **TELKOMNIKA** Telecommunication Computing Electronics and Control, vol. 20, no. 1, pp. 221-234.
- [21] Rao M., Ranjan R., Kashyap N., Sarin R.K. (2021). "Performance Analysis of Normally-on Dual Gate Algan/Gan Hemt," Transactions on Electrical and Electronic Materials, 1-9.

- [22] JADLI, Utkarsh. (2021). Modeling Power GaN-HEMTs Using Standard MOSFET Equations and Parameters in SPICE. Electronics, 10.2: 130.
- [23] Dimitrijev S. (2012). MOSFET. Principles of Semiconductor Devices, 2nd ed.; Oxford University Press: New York, NY, USA, 312–316.
- [24] Garcia F, Shamsir S., Islam S. (2018). A SPICE Model for GaN-Gate Injection Transistor (GIT) at Room Temperature, Connecticut Symposium on Microelectronics & Optoelectronics.
- [25] Liu, X., Liu, B, Low, E. K. F, Chin, H.-C, Liu, W, Yang, M. (2010). Diamond-like carbon (DLC) liner with highly compressive stress formed on AlGaN/GaN MOS-HEMTs with in situ silane surface passivation for performance enhancement, IEEE International Electron Device Meeting 2010, San Francisco CA, 11.3.1 11.3.4.